

Choice of Observing Schedules for Astrometric Planet Searches

Eric B. Ford¹

Astronomy Department, 601 Campbell Hall, University of California at Berkeley, Berkeley,
CA 94720-3411, USA

eford@astron.berkeley.edu

Received _____; accepted _____

draft

¹Miller Research Fellow

ABSTRACT

The Space Interferometry Mission (SIM) will make precise astrometric measurements that can be used to detect planets around nearby stars. Since observational time will be extremely valuable, it is important to consider how the choice of the observing schedule influences the efficiency of SIM planet searches. We have conducted Monte Carlo simulations of astrometric observations to understand the effects of different scheduling algorithms. We find that the efficiency of planet searches is relatively insensitive to the observing schedule for most reasonable observing schedules.

Subject headings: planetary systems – techniques: interferometric

1. Introduction

The discovery of ~ 130 extrasolar planets via radial velocity surveys (Butler *et al.* 2002 and references therein; <http://exoplanets.org>) has challenged theories of planet formation and evolution. While radial velocity surveys are most sensitive to planets in short-period orbits around lower main-sequence stars, astrometric surveys are most sensitive to planets in long-period orbits, up to the duration of the survey. Thus, radial velocity and astrometric surveys could be complementary for studying extrasolar planetary systems.

The flagship astrometric survey for extrasolar planets in the next decade is the Space Interferometry Mission, SIM (<http://sim.jpl.nasa.gov/>). Two SIM key projects will search for low-mass extrasolar planets around nearby stars (Marcy *et al.* 2002; Shao *et al.* 2002). SIM is expected to make targeted observations with a precision of $\sim 1 \mu\text{as}$ for differential astrometry. The relatively small number of targeted observations (~ 4500 two dimensional measurements with $1\mu\text{as}$ precision over a 5 year mission if 10% of the time is devoted to planet searches) dictates that care should be taken to maximize the value of the available observing time. In this paper, we explore how the choice of observing schedule affects the efficiency of an astrometric planet search, such as SIM. While the detailed results would inevitably differ for radial velocity surveys, we expect that the main conclusions are likely to apply to radial velocity surveys as well as other pointed astrometric surveys. Our results will not be useful for non-pointed astrometric missions, such as GAIA, which must adhere to a fixed scanning pattern determined by the rotation and orbit of the satellite (Lattanzi *et al.* 2000).

We describe our assumptions and methods in §2. In §3 we present the results of our simulations. In §4 we summarize our main findings and conclusions.

2. Methods

The two studies of Sozzetti *et al.* (2002) and Ford & Tremaine (2003) simulated SIM observations and arrived at similar detection criteria when stated in terms of the scaled signal (see Eq. 2 below), despite the fact that Sozzetti *et al.* (2002) assumed relative astrometry using three reference stars while Ford & Tremaine (2003) modeled astrometry relative to a fixed reference frame. Thus, we consider only absolute astrometric measurements of the target star, neglecting potential complications due to the parallax and proper motion of reference stars. We expect that our results can be simply applied to SIM’s narrow angle planet search as well as most other astrometric planet searches.

2.1. Model Planets and Observations

We simulated astrometric observations of many hypothetical stars. Each star is assigned a position (RA , Dec), distance (D), proper motion ($\vec{v_\perp}/D$), mass (M), and a single planet. The stellar positions are distributed uniformly in a sphere of radius 20 parsecs centered on the Sun, except that we reject any stars within 1 parsec of the Sun. The stellar velocities are drawn from a three dimensional Gaussian distribution with mean 0 km s^{-1} and standard deviation 40 km s^{-1} in each direction. The stellar masses are set to $1M_\odot$ and the stellar velocities are randomly directed in space.

Each planet is assigned a mass (m), orbital period (P), orbital eccentricity (e), inclination of the orbital plane to the plane of the sky (i), argument of pericenter (ω), longitude of ascending node (Ω), and mean anomaly at a specified time (M_o). The planetary mass and orbital period are drawn from the mass-period distribution of Tabachnik & Tremaine (2002), with masses ranging from one Earth mass ($1M_\oplus$) to ten Jupiter masses ($10M_{Jup}$) and orbital periods ranging from 2 days up to the duration of the astrometric

survey (P_{SD}). The eccentricities are drawn from a uniform distribution between 0 and 1. The orbits are randomly oriented in space.

A planet in a circular orbit will cause the star to move on the plane of the sky with a semi-amplitude,

$$\frac{\alpha}{''} \equiv \frac{m}{M} \frac{a}{\text{AU}} \frac{\text{pc}}{D}. \quad (1)$$

We present our results in terms of the “scaled signal”,

$$S \equiv \frac{\alpha}{\sigma_d}, \quad (2)$$

where σ_d is the single measurement precision for a one dimensional measurement of the position of the star. For SIM, the single measurement precision would be the precision obtained by combining multiple one dimensional relative delay measurements between the target star and each reference star during a single observing visit. In our simulations, we set $\sigma_d = 1\mu\text{as}$, but many of our results can be scaled to different σ_d and our conclusions are not sensitive to the value of σ_d .

For each star we simulated $2N_{obs} = 96$ one dimensional astrometric observations grouped in pairs. Each pair of observations occurs nearly simultaneously and is made with perpendicular baselines. The N_{obs} observation times (t_i) are spread over the survey duration $P_{SD} = 10$ years (although at present the nominal SIM lifetime is only 5 years). We will consider several different methods for choosing the observing times in §3.

2.2. Data Analysis

For each set of simulated observations, first, we attempt to fit a no-planet model which includes only the star’s five astrometric parameters (π , RA , Dec , and the two components of \vec{v}). The parallax, π is the inverse of the distance to the star (measured in parsecs). To carry out the fit, we use the Levenberg-Marquardt algorithm (Press *et al.* 1992) combined

with a good initial guess of the astrometric parameters. By “good” we mean that the initial guess for the star’s distance and velocity to within $\sim 1\%$ of their true values and the star’s position is the weighted average of the observations.

After identifying the best-fit astrometric parameters, we calculate the usual sum of squares of the residuals (χ^2_0) to evaluate the appropriateness of the no-planet model. If a χ^2 test can reject the no-planet model with 99.9% confidence, then we proceed to fit a model which includes a planet. We attempt to find the best-fit one-planet model using the Levenberg-Marquart algorithm with good initial guesses ($\sim 1\%$ dispersion about the true values) for the astrometric parameters and the planet’s orbital parameters. We hold the star’s mass fixed at its actual value. If the χ^2 statistic for the best-fit one-planet model (χ^2_1) is significantly less than χ^2_0 (the best-fit for the no-planet model) according to an F -test, then we consider the planet to be detected. The fitting is done most efficiently by using the Thiele-Innes coordinates,

$$X_1 = a_* [\cos \omega \sin \Omega + \sin \omega \cos \Omega \cos i] / D \quad (3)$$

$$Y_1 = a_* [\cos \omega \cos \Omega - \sin \omega \sin \Omega \cos i] / D \quad (4)$$

$$X_2 = a_* [-\sin \omega \sin \Omega + \cos \omega \cos \Omega \cos i] / D \quad (5)$$

$$Y_2 = a_* [-\sin \omega \cos \Omega - \cos \omega \sin \Omega \cos i] / D, \quad (6)$$

where a_* is the star’s semi-major axis. After finding the best-fit Thiele-Innes coordinates, we convert these to conventional orbital elements. The planet’s semi-major axis is determined by $a = a_* M/m$, and the planet’s mass is determined by

$$\frac{m/M}{(1 + m/M)^{2/3}} = \frac{a_*}{\left(\frac{G}{4\pi^2} M\right)^{1/3} P^{2/3}}, \quad (7)$$

where G is the gravitational constant and the equation is solved iteratively. Since we use very good initial guesses as inputs to the local minimization algorithm, the accuracy of our mass and orbit determinations is optimistic. For actual systems, it will be necessary to

perform a global search which may result in even larger errors when estimating a planet’s mass and orbital parameters. We have not performed a global search, as that would make it impractical to conduct such a large number of simulations as performed in this paper. The ability of such global searches to converge on the correct solution is poorly understood and worthy of separate investigation.

We repeat these calculations for hundreds of thousands of stars to determine the fraction of planets which can be detected with the various observing schedules considered. We also investigate the fraction of planets whose mass and/or orbital elements are accurately measured.

2.3. Observing Schedules

The previous study of Sozzetti *et al.* (2002) calculated the sensitivity of SIM for detecting extrasolar planets and included a comparison of a few possible observing schedules. In this study, we examine a much larger list of possible observing schedules.

We consider several possible observing schedules:

1. Regular Periodic: constant spacing, Δt ,
2. Golomb Ruler: times proportional to marks on shortest known Golomb ruler with N_{obs} marks,
3. Regular Power Law: times proportional to the observation number raised to a power ($t_i \sim i^\beta$),
4. Regular Logarithmic: times proportional to logarithm of observation number ($t_i \sim \log i$) with minimum spacing, Δt_{min} ,

5. Regular Geometric: times proportional to a constant raised to the power of the observation number ($t_i \sim \beta^i$) with minimum spacing Δt_{min} ,
6. Random Uniform: random times uniform in t ,
7. Random Power Law: random times uniform in t^β ,
8. Random Logarithmic: random times uniform in $\log t$ with minimum spacing Δt_{min} , and
9. Periodic with Perturbation: constant spacing Δt_0 , but with a random Gaussian perturbation with zero mean and standard deviation $\epsilon \Delta t_0$.

A Golomb ruler is a sequence of integers which can be considered as the distance to the next mark on a ruler such that the distance between each pair of marks is a unique integer. That is

$$\Delta_{pq} = G_q - G_p \quad (8)$$

is unique for each pair of p and q , where $1 \leq p < q \leq N_{obs}$. The shortest known Golomb ruler for a given number of marks can provide a good basis for designing a linear interferometer (Robinson & Bernstein 1967), because it includes as many distinct baselines as possible. We consider observing schedules based on Golomb rulers to see if such schedules are advantageous for reconstructing planetary orbits. Observing schedule #2 places observations at times $t_i = G_i P_{SD}/N_G$, where P_{SD} is the survey duration, G_i is the distance to the i -th mark on the shortest known Golomb ruler with N_{obs} marks, and N_G is the length of the Golomb ruler.

Observing schedules #3-5 and #7-9 have a single free parameter. We consider multiple values for these parameters.

3. Results

For each observing strategy we have simulated observations of many stars with a planet to determine the efficiency of the observing schedule for detecting planets and for measuring their masses and orbital parameters.

3.1. Overall Rates

First, we compare the total number of planet detections when using each of several different observing schedules. In Table 1, columns 2 and 3, we list the fraction of planets which are detected for each observing schedule, averaging over all planet masses ($1M_{\oplus} - 10M_{Jup}$), orbital periods (2 d-10 yr), and other parameters. Table 2 is similar to Table 1, but only includes planets with masses between $1M_{\oplus}$ and $20M_{\oplus}$. Despite the wide variety of observing schedules considered, all of the schedules that we consider detect planets at very similar rates.

Next, we consider the fraction of planets for which masses and orbits are measured with 30% and 10% accuracy (Tables 1 and 2, columns 4-7). Again, most of the observing strategies measure masses and orbits at very similar rates. Since the mass is a function of only the orbital period and amplitude, measuring the mass is somewhat easier than measuring all of the orbital parameters to the same precision.

In Figs. 1-5, we show the rates of detecting planets and measuring their masses and orbits. The upper left hand panel is for detections, the upper right hand panel is for measuring the mass with 30% accuracy, the lower left panel is for measuring the orbit with 30% accuracy, and the lower right panel is for measuring the orbit with 10% accuracy. In each of these figures, the different line styles are for simulations using different observing schedules (solid, periodic; dotted, periodic with perturbations ($\epsilon = 0.2$); dot-long dash,

logarithmic ($\Delta t_{min} = 30$ d); short dash, power law ($\beta = 0.5$); dot-short dash, geometric ($\Delta t_{min} = 30$ d); short dash-long dash, Golomb ruler). The various curves are often difficult to distinguish, reflecting the fact that most of the observing schedules that we consider have very similar efficiencies for detecting and characterizing planets. We now discuss each figure in turn.

3.2. Rate versus Scaled Signal

In Fig. 1, we investigate how the rates of detecting planets and measuring their masses and orbits depend on the scaled signal, S , averaging over orbital periods, eccentricities, and other parameters. Clearly, planets will not be detected for sufficiently small S , and will be easy to detect and characterize for sufficiently large S . While there is a 50% probability of measuring an orbit with 10% accuracy for a planet with a modest scaled signal ($S \simeq 6$), a significantly larger scaled signal ($S \simeq 30$) is required for there to be a 95% probability of measuring the orbit with the same accuracy, as noted in Ford and Tremaine (2003). While this paper will focus on the difference between the rates of detection and characterization for different observing schedules, it is important to realize that all of the observing schedules that we consider perform very similarly (see Fig. 1).

3.3. Rate versus Orbital Period

Next, we investigate how the rates of detecting planets and measuring their masses and orbits depends on the orbital period, P , averaging over a distribution of planet masses based on the observed radial velocity planets (Tabachnik and Tremaine 2002). Planets with very short period orbits are typically difficult to detect, primarily due to the smaller scaled signal, S (see Fig. 2).

In Fig. 3, we plot the rates for detecting planets and measuring their masses and orbits as a function of orbital period, while fixing the scaled signal, $S = 6$. Since the scaled signal is held constant for all orbital periods, the rates are higher than in Fig. 2 for planets with small orbital periods, but smaller for planet with long orbital periods. Note that there is a sharp decline in rates for measuring masses and orbits for planets with orbital periods approaching the duration of the astrometric survey. The regular periodic (solid line) and periodic with perturbations (dotted line) observing schedules performed marginally better for planets with long orbital periods and the geometric strategy performed worst.

In Fig. 3, the regular periodic observing schedule (solid line) reveals other features. The reduction in the rates of detecting planets and measuring their masses and orbital periods near ~ 0.2 yr (and to a lesser extent at harmonics of this period) for the regular periodic observing schedule is due to aliasing. We will address this issue further in §3.8. Also, note that the regular periodic observing schedule is significantly less efficient at detecting and measuring the mass of planets with very small orbital periods, due to the lack of pairs of observations with small spacings.

3.4. Rate versus Orbital Eccentricity

In Fig. 4, we show the rates of detecting planets and measuring their masses and orbits as a function of orbital eccentricity for fixed scaled signal, $S = 4$, and orbital period, $P = 2.5$ yr. All the observing strategies which we consider have a similar functional form and have a significantly lower rate of characterizing planets with high eccentricities. As the orbital period approaches the duration of observations, the effect becomes significant at smaller eccentricities. This should be expected due to projection effects. For a star perturbed by a single planet, the star will appear to trace out an ellipse with semi-major and semi-minor axes proportional to $S\sqrt{1 - e^2 \sin^2 \omega}$ and $S\sqrt{1 - e^2 \cos^2 \omega} |\cos i|$. Planets

with large eccentricities will sometimes be harder to detect (i.e., when the major axis of the orbit is nearly parallel to the line of sight).

3.5. Rate versus Inclination

The efficiency of detecting and characterizing planets also depends on the inclination of the planet’s orbit relative to the plane of the sky (Sozzetti *et al.* 2001, 2002, 2003; Eisner & Kulkarni 2001, 2002). If a planet’s orbit is exactly edge-on, then the projected motion of the star is confined to one dimension. When the baseline of the interferometer is perpendicular to the orbital plane, observations provides no information about the orbit. If the projected orbital plane and interferometer baseline differ by an angle, θ , then the amplitude of the signal is reduced by a factor $|\cos i|$. In Fig. 5, we show the rates for detecting planets and measuring their masses and orbits as a function of the inclination for a fixed scaled signal, $S = 2$, averaging over the other parameters. As expected, all the observing strategies which we consider have a similar functional form and have a slightly lower rate of characterizing planets which are viewed nearly edge-on (small $\cos i$). The effect becomes less significant for larger scaled signals. This should be expected due to projection effects. For small scaled signal, the inclination effect can result in a significantly reduced efficiency for detecting a planets for a wide range of orbital inclinations. When the scaled signal is large, the effect is significant only for orbits which are very close to $\cos i = 0$.

3.6. Regular versus Random Observing Schedules

Next, we compare regular and random observing schedules. In Fig. 6 we show the rates of detecting planets and measuring their masses and orbits as a function of orbital period for fixed S . The solid lines show the results for observing schedules with regular spacings

and the dotted lines show the results for observing schedules with random observing times drawn from a distribution based on the regular observing schedule shown in the same panel. The left column is for regular periodic (solid), random uniform (dashed), and periodic with perturbations ($\epsilon = 0.2$, dotted) observing schedules. The middle column is for regular logarithmic (solid) and random logarithmic (dotted) observing schedules with $\Delta t_{min} = 30$ d. The right column is for regular power law (solid) and random power law (dotted) with $\beta = 0.5$. The top row is for detecting the planet (assuming $S = 2$), the middle row is for measuring the planetary mass with 30% accuracy (assuming $S = 4$), and the bottom row is for measuring the planet’s orbit with 10% accuracy (assuming $S = 6$).

In most cases, the random version of the observing schedules performs slightly less well than the similar regular observing schedule, especially for orbital periods approaching the duration of the astrometric survey. This is typical because the random schedules sometimes contain a larger gap between observations than would occur in the similar regular observing schedule.

One notable exception occurs for the regular periodic observing schedule (left column, solid line). Since regular periodic spacings result in significant aliasing, adding randomness improves the efficiency. However, a uniform random schedule (left column, dashed line) also suffers somewhat at long orbital periods, as described above. An alternative solution to the aliasing problem is to construct an observing schedule by starting with equal periodic spacings and then adding a Gaussian perturbation to each observing time (left column, dotted line). We explore this possibility further in §3.8.

3.7. Rate versus Minimum Spacing

For each type of regular observing schedule that we considered, the rates of detecting planets and measuring their masses and orbits increased as the minimum spacing was increased, and the observing schedule became more similar to the schedule with regular periodic spacings. As an example of this effect, we show the results for observing schedules using geometric observing schedules with different minimum spacings in Fig. 7. The upper left panel is for detecting a planet, the upper right panel is for measuring the mass with 30% accuracy, the lower left panel is for measuring the orbit with 30% accuracy, and the bottom right panel is for measuring the orbital parameters with 10% accuracy. The different line styles are for simulations using geometric observing schedules with different minimum spacings, Δt_{min} (solid, 1d; dotted, 3d; long dash, 6d; dot-long dash, 10d; short dash, 30d; dot-short dash, 60d).

We find that there is reduced efficiency for observing schedules with small Δt_{min} , consistent with the findings of Sozzetti *et al.* (2002). Since the total number of observations and the survey duration are held constant, observing schedules with some closely spaced observations (small Δt_{min}) also result in some large gaps between other observations. This reduces the sensitivity to planets with orbital periods approaching the duration of the survey. There is a similar effect for observing schedules using logarithmic or power law spacings between observations.

3.8. Aliasing

An observing schedule with constant spacing between observations (Fig. 8, solid line) will obviously have difficulty detecting planets whose orbital period is nearly equal to the time between observations. Yet, observing with a uniform spacing (Δt) between

observations gives one of the highest overall rates of planet detection. A variant on this is an observing schedule in which the observing times are perturbed by a normal random variable (with standard deviation equal to $\epsilon\Delta t$).

In Fig. 8, we show the rates of detecting planets and measuring their masses and orbits as a function of orbital period for fixed S . Here we have zoomed in to examine more closely rates for detecting and characterizing planets with orbital periods near $10\text{yr}/48 \simeq 0.2$ yr, where aliasing is most significant. The harmonic at 0.1 yr can also be seen in this figure. The solid lines are for a regular periodic observing schedule, while the other lines are for a periodic with perturbations observing schedule with different values of ϵ . The upper left panel is for detecting a planet ($S = 4$), the upper right panel is for measuring the mass with 30% accuracy ($S = 4$), the lower left panel is for measuring the orbit with 30% accuracy ($S = 6$), and the bottom right panel is for measuring the orbital parameters with 10% accuracy ($S = 8$).

In each panel, the periodic with perturbations observing schedule significantly reduces the severity of the aliasing for $\epsilon \geq 0.1$ (dot-long dash line) and virtually eliminated the effect for $\epsilon \simeq 0.4$ (dot-short dash line). This results in an slightly higher overall rate of planet detections, and makes the periodic with perturbations observing schedule the best schedule that we have examined.

3.9. Parallax Effect

Parallax causes nearby stars to appear to trace out an ellipse on the sky similar to (but typically much larger than) the perturbation caused by a planetary mass companion. Since the period of the parallax effect is one year, planets with orbital periods nearly equal to one year are more difficult to detect (Lattanzi *et al.* 2000; Sozzetti *et al.* 2002).

In Fig. 9, we show the rates of detecting planets and measuring their masses and orbits as a function of orbital period for fixed S . We have zoomed in to examine more closely planets with orbital periods near 1 yr. The upper left panel is for detecting a planet ($S = 2$), the upper right panel is for measuring the mass with 30% accuracy ($S = 4$), the lower left panel is for measuring the orbit with 30% accuracy ($S = 6$), and the bottom right panel is for measuring the orbital parameters with 10% accuracy ($S = 8$). The different line styles are for simulations using different observing schedules.

While there is a small but significant decrease ($\sim 30\%$ for $S = 2$) in the detection rate near $P \simeq 1$ year, the rate for measuring masses or orbits with 10% accuracy is only slightly affected. The choice of observing schedule does not significantly change the parallax effect.

4. Discussion

We have considered several possible observing schedules for a targeted astrometric planet search similar to SIM. For most reasonable observing schedules, the efficiency of planet searches is relatively insensitive to the observing schedule. Note that we have used local fitting algorithms which rely on good initial estimates of the astrometric and orbital parameters and have not explored possible problems associated with converging to the correct global solution.

Observing strategies which do not include observations with spacings less than a planet’s orbital period have some difficulty measuring the orbital parameters accurately. However, since the amplitude of the astrometric perturbations scales with $P^{2/3}$, any astrometric planet search will have trouble detecting very short period planets in any case.

Since the number of observations is held constant, observing schedules which concentrate too many of their observations in a short period of time have difficulty

accurately measuring orbits for longer period systems. This effect favors observing schedules which avoid large gaps between observations. All of the regular observing schedules which we consider can be highly competitive, provided that the minimum spacing is sufficiently large (≥ 20 d). For these observing schedules, the minimum spacing is only a factor of a few less than the average spacing between observations ($\simeq 76$ d $\simeq 0.2$ yr).

Observing schedules with observing times drawn randomly from a broad probability distribution typically resulted in slightly poorer rates for detecting and characterizing planets with orbital periods approaching the duration of the astrometric survey. This is a result of occasional large gaps between observing times. However, drawing all observation times randomly from a uniform distribution was only slightly less efficient than the best performing observing schedules that we considered.

While aliasing is very strong for an observing schedule with regular periodic observations, the aliasing can be significantly reduced or virtually eliminated by applying a Gaussian perturbation to the observing times with fractional standard deviation $\sim 10 - 40\%$ (for $N_{obs} = 48$). This also improves the rates of detection and characterization for planets with small orbital periods. The magnitude of the perturbation necessary is expected to scale as $\sim 1/N_{obs}$ based on Fourier theory.

Planet searches will also be less sensitive to planets with orbital periods nearly equal to a year due to the parallax effect. The fact that this effect occurs near orbital periods of $\simeq 1$ year is unfortunate, since this is near the range of orbital periods of particular interest due to the possibility of planets in the habitable zone of another solar-type stars. However, for stars of other spectral types (and hence luminosities), the habitable zone is expected to occupy different orbital periods, while the parallax effect always occurs near orbital periods of one year. In any case, the choice of observing schedule does not significantly reduce the significance of the parallax effect.

Of the observing schedules which we have considered, we find there is a small advantage in terms of the rate of detecting planets and measuring their orbits for an observing schedule obtained by starting with an equal spacing between observations and adding a small perturbation ($\simeq 0.4$) to each observing time. Note that all of the observing schedules which we have considered are fixed in advance of all observations. We have performed additional calculations for $2N_{obs} = 48$ and verified that our conclusions for the efficiency of one observing schedule relative to another were not significantly changed. In the future, we hope to study the potential benefits of algorithms which incorporate knowledge gained from previous observations. In particular, preliminary results suggest that significant increases in efficiency are possible by allowing the number of observations of each target to vary depending on the outcome of the previous observations. If it is also possible to choose the time of additional observations, then even further improvements in efficiency are likely possible (Ford 2005).

Finally, we emphasize that the differences between observing schedules which we have identified are relatively small. This conclusion has significant implications for planning an astrometric planet search such as SIM. Since the exact scheduling of observation times is not critical, it may be advantageous to schedule observations so as to minimize time associated with mission overhead (e.g., measuring grid and reference stars, slewing), allowing a greater number of observations per target star or a greater number of stars to be surveyed.

We thank Scott Tremaine for his guidance and an anonymous referee for their suggestions. This research was supported in part by NASA grant NAG5-10456, the EPICs SIM Key Project, and the Miller Institute for Basic Research.

REFERENCES

Butler, R.P., Marcy, G.W., Vogt, S.S., Tinney, C.G., Jones, H.R.A., McCarthy, C., Penny, A.J., Apps, K., Carter, B.D. 2002, *ApJ*, 578, 565.

Eisner, J.A. & Kulkarni, S.R. 2001, *ApJ*, 561, 1107

Eisner, J.A. & Kulkarni, S.R. 2002, *ApJ*, 574, 426.

Ford, E.B. & Tremaine, S. 2003 *PASP*, 115, 1171.

Ford, E.B. 2005, in preparation.

Lattanzi, M.G., Spagna, A., Sozzetti, A., Casertano, S. 2000, *MNRAS*, 317, 211.

Marcy, G. et al. 2002 Discovery of Planetary Systems with SIM proposal,
http://planetquest.jpl.nasa.gov/SIM/science_marcy.pdf

Press, W. H., Teukolsky, S. A., Vetterling, W. T., & Flannery, B. P. 1992, *Numerical Recipes in C: the Art of Scientific Computing*. New York: Cambridge University Press.

Robinson, J.P. & Bernstein, A.J. 1967, *IEEE Transactions on Information Theory*, IT-13.

Shao, M. et al. 2002 Extrasolar Planet Interferometric Survey proposal,
http://planetquest.jpl.nasa.gov/SIM/science_shao.pdf

Sozzetti, A., Casertano, S., Lattanzi, M.G., Spagna, A. 2001, *A&A* 373, 21.

Sozzetti, A., Casertano, S., Brown, R.A., Lattanzi, M.G. 2002, *PASP*, 114, 117.

Sozzetti, A., Casertano, S., Brown, R.A., Lattanzi, M.G. 2003, *PASP*, 116, 1072.

Tabachnik, S. & Tremaine, S. 2002, *MNRAS*, 335, 151.

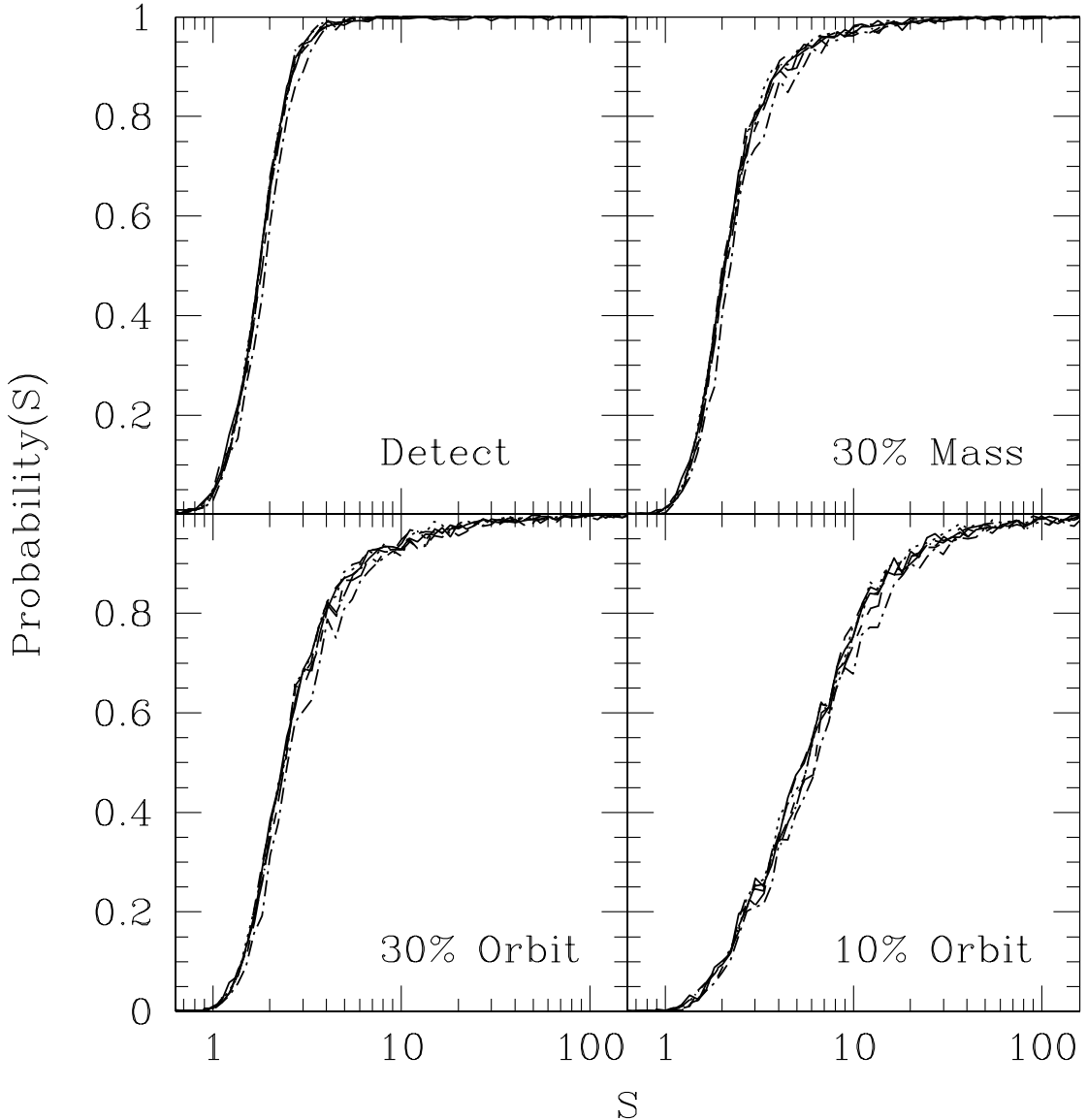


Fig. 1.— In each panel we show the probability for detecting a planet or measuring its mass or orbit as a function of the scaled signal, S , averaging over orbital periods, eccentricities, and other parameters. The upper left panel is for detecting a planet, the upper right panel is for measuring the mass with 30% accuracy, the lower left panel is for measuring the orbit with 30% accuracy, and the bottom right panel is for measuring the orbital parameters with 10% accuracy. The different line styles are for simulations using different observing schedules (solid, periodic; dotted, periodic with perturbations ($\epsilon = 0.2$); dot-long dash, logarithmic ($\Delta t_{min} = 30$ d); short dash, power law ($\beta = 0.5$); dot-short dash, geometric ($\Delta t_{min} = 30$ d); short dash-long dash, Golomb ruler). It is clear that our choice of observing schedule has

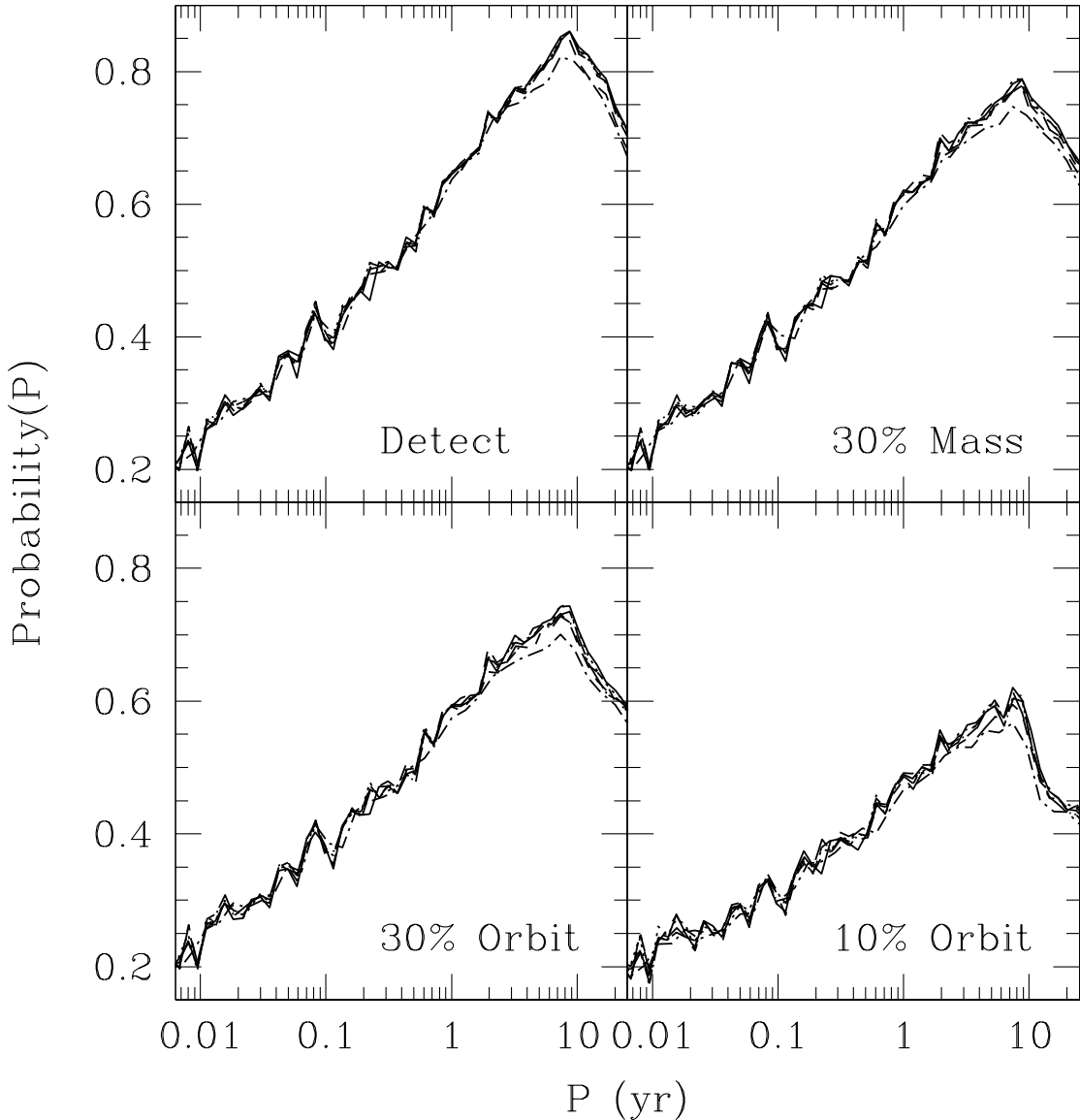


Fig. 2.— In each panel we show the probability for detecting a planet or measuring its mass or orbit as a function of the orbital period, P , averaging over planet mass, eccentricities, and other parameters. The upper left panel is for detecting a planet, the upper right panel is for measuring the mass with 30% accuracy, the lower left panel is for measuring the orbit with 30% accuracy, and the bottom right panel is for measuring the orbital parameters with 10% accuracy. The different line styles are for simulations using different observing schedules (solid, periodic; dotted, periodic with perturbations ($\epsilon = 0.2$); dot-long dash, logarithmic ($\Delta t_{min} = 30$ d); short dash, power law ($\beta = 0.5$); dot-short dash, geometric ($\Delta t_{min} = 30$ d); short dash-long dash, Golomb ruler). For all sensible observing schedules, astrometric

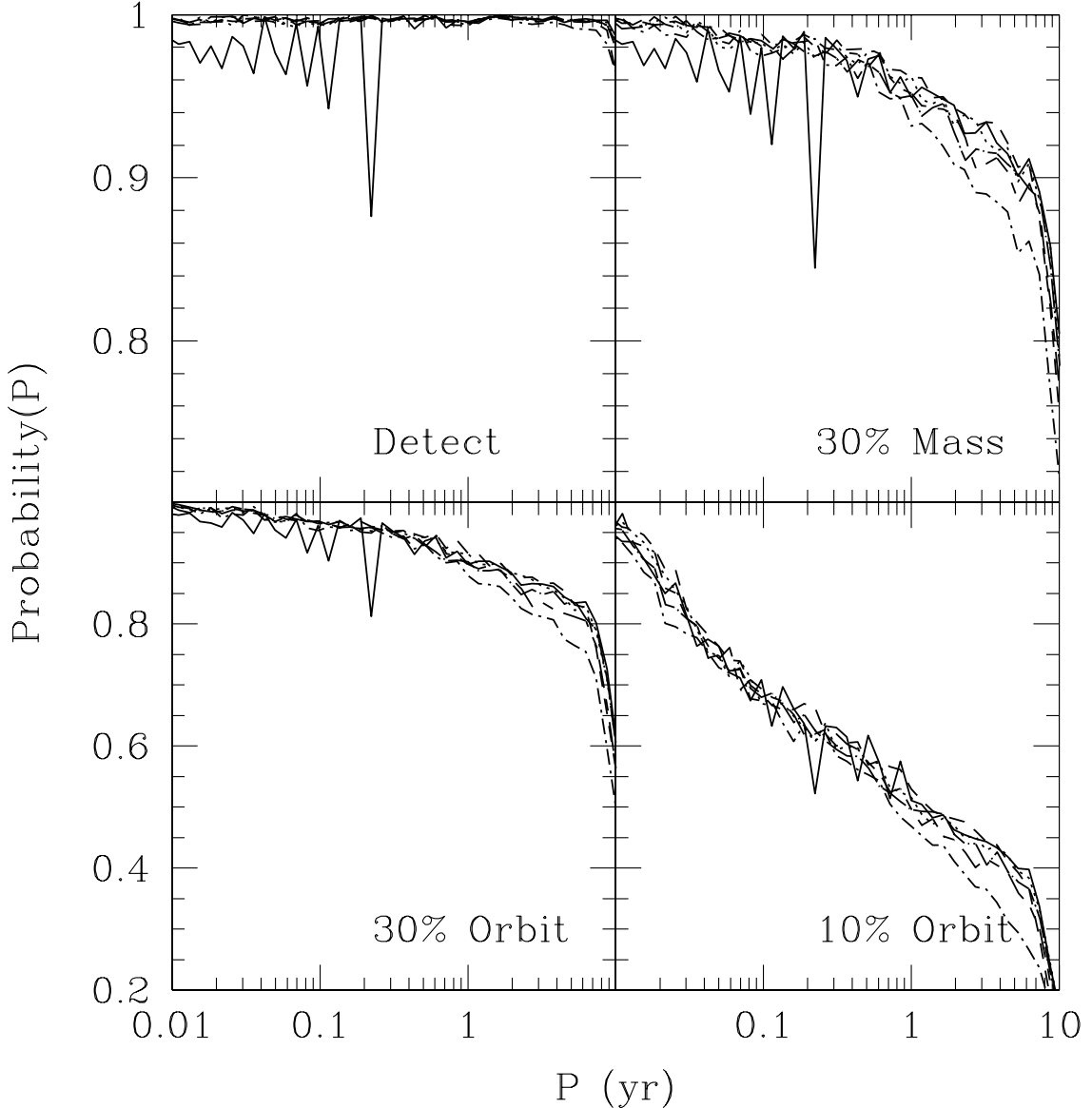


Fig. 3.— In each panel we show the probability for detecting a planet or measuring its mass or orbit as a function of the orbital period, P , for a fixed scaled signal, $S = 6$, averaging over the eccentricities, and other parameters. The upper left panel is for detecting a planet, the upper right panel is for measuring the mass with 30% accuracy, the lower left panel is for measuring the orbit with 30% accuracy, and the bottom right panel is for measuring the orbital parameters with 10% accuracy. The different line styles are for simulations using different observing schedules (solid, periodic; dotted, periodic with perturbations ($\epsilon = 0.2$); dot-long dash, logarithmic ($\Delta t_{min} = 30$ d); short dash, power law ($\beta = 0.5$); dot-short dash, geometric ($\Delta t_{min} = 30$ d); short dash-long dash, Golomb ruler). There are significant

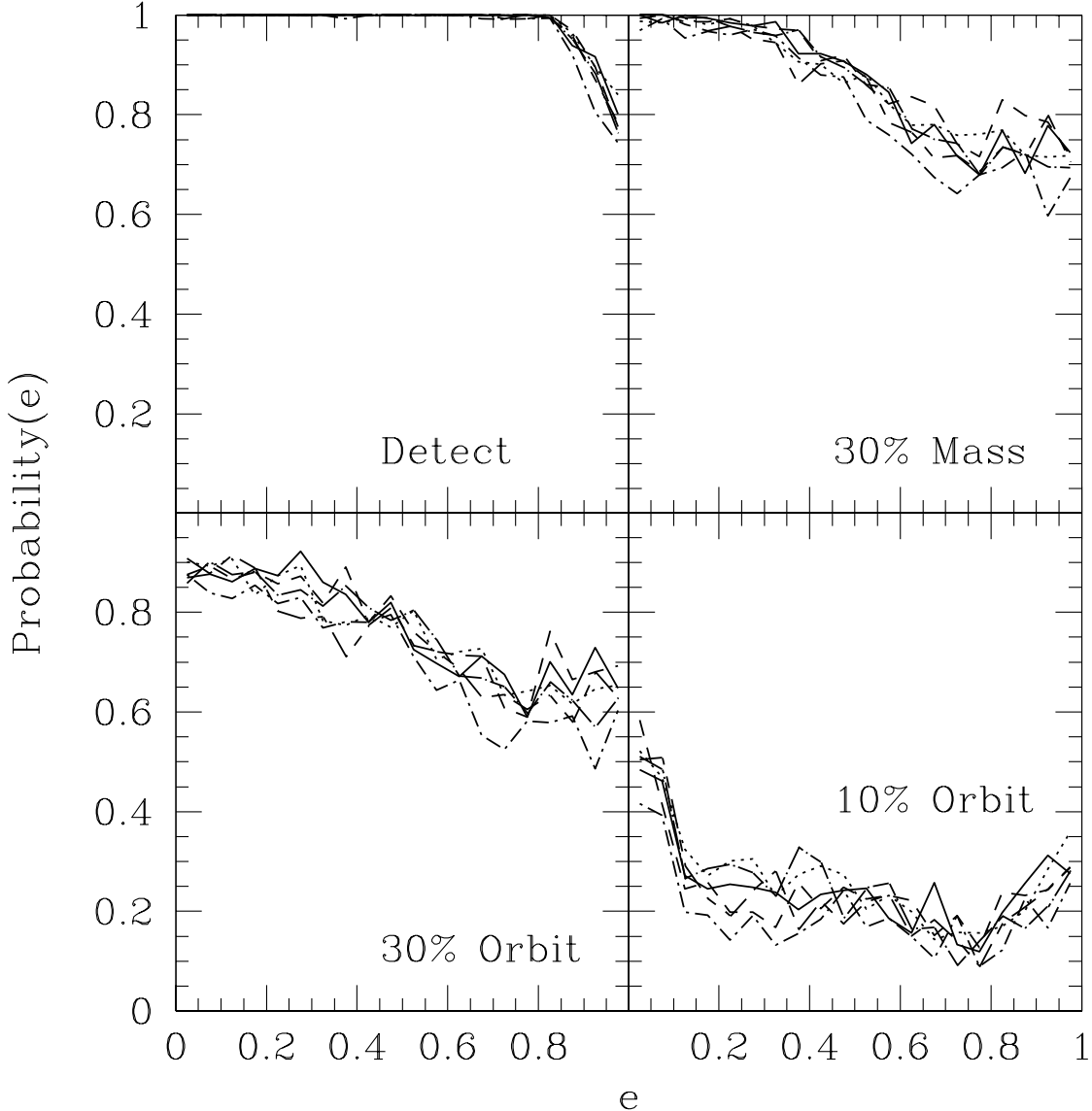


Fig. 4.— In each panel we show the probability for detecting a planet or measuring its mass or orbit as a function of the orbital eccentricity, e , for a fixed scaled signal, $S = 6$, and orbital period, $P = 2.5$ yr, averaging over the other parameters. The upper left panel is for detecting a planet, the upper right panel is for measuring the mass with 30% accuracy, the lower left panel is for measuring the orbit with 30% accuracy, and the bottom right panel is for measuring the orbital parameters with 10% accuracy. The different line styles are for simulations using different observing schedules (solid, periodic; dotted, periodic with perturbations ($\epsilon = 0.2$); dot-long dash, logarithmic ($\Delta t_{min} = 30$ d); short dash, power law ($\beta = 0.5$); dot-short dash, geometric ($\Delta t_{min} = 30$ d); short dash-long dash, Golomb ruler).

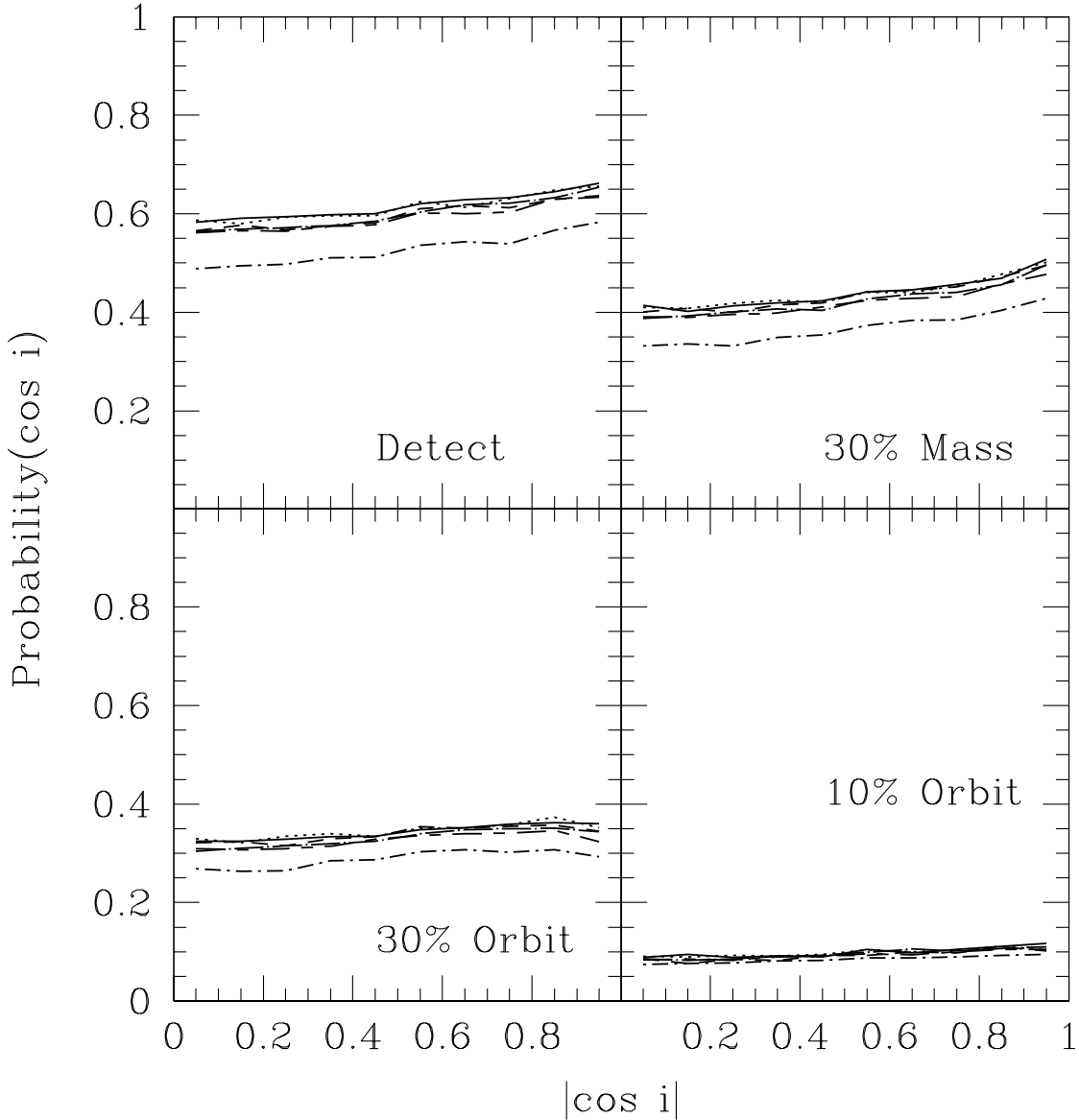


Fig. 5.— In each panel we show the probability for detecting a planet or measuring its mass or orbit as a function of the cosine of the inclination to the plane of the sky, $\cos i$, for a fixed scaled signal, $S = 2$, averaging over the other parameters. The upper left panel is for detecting a planet, the upper right panel is for measuring the mass with 30% accuracy, the lower left panel is for measuring the orbit with 30% accuracy, and the bottom right panel is for measuring the orbital parameters with 10% accuracy. The different line styles are for simulations using different observing schedules (solid, periodic; dotted, periodic with perturbations ($\epsilon = 0.2$); dot-long dash, logarithmic ($\Delta t_{min} = 30$ d); short dash, power law ($\beta = 0.5$); dot-short dash, geometric ($\Delta t_{min} = 30$ d); short dash-long dash, Golomb ruler).

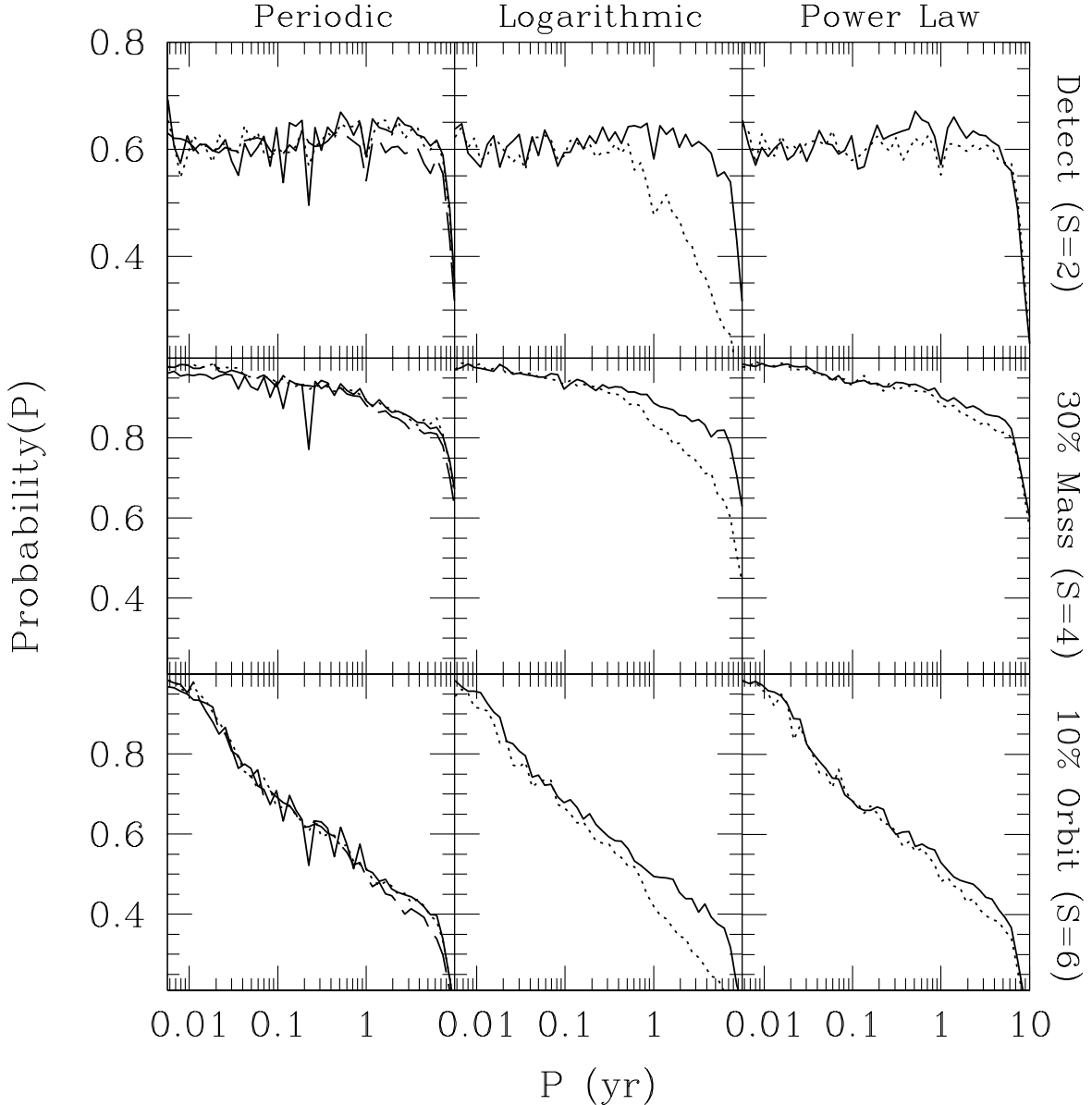


Fig. 6.— In each panel we show the probability for detecting a planet or measuring its mass or orbit as a function of the orbital period, P , for a fixed scaled signal, S , averaging over the other parameters. The left column is for regular periodic (solid), random uniform (dashed), and periodic with perturbations ($\epsilon = 0.2$, dotted) observing schedules. The middle column is for regular logarithmic (solid) and random logarithmic (dotted) observing schedules with $\Delta t_{min} = 30$ d. The right column is for regular power law (solid) and random power law (dotted) with $\beta = 0.5$. The top row is for detecting the planet (assuming $S = 2$), the middle row is for measuring the planetary mass to with 30% accuracy (assuming $S = 4$), and the bottom row is for measuring the planet's orbit with 10% accuracy (assuming $S = 6$). In

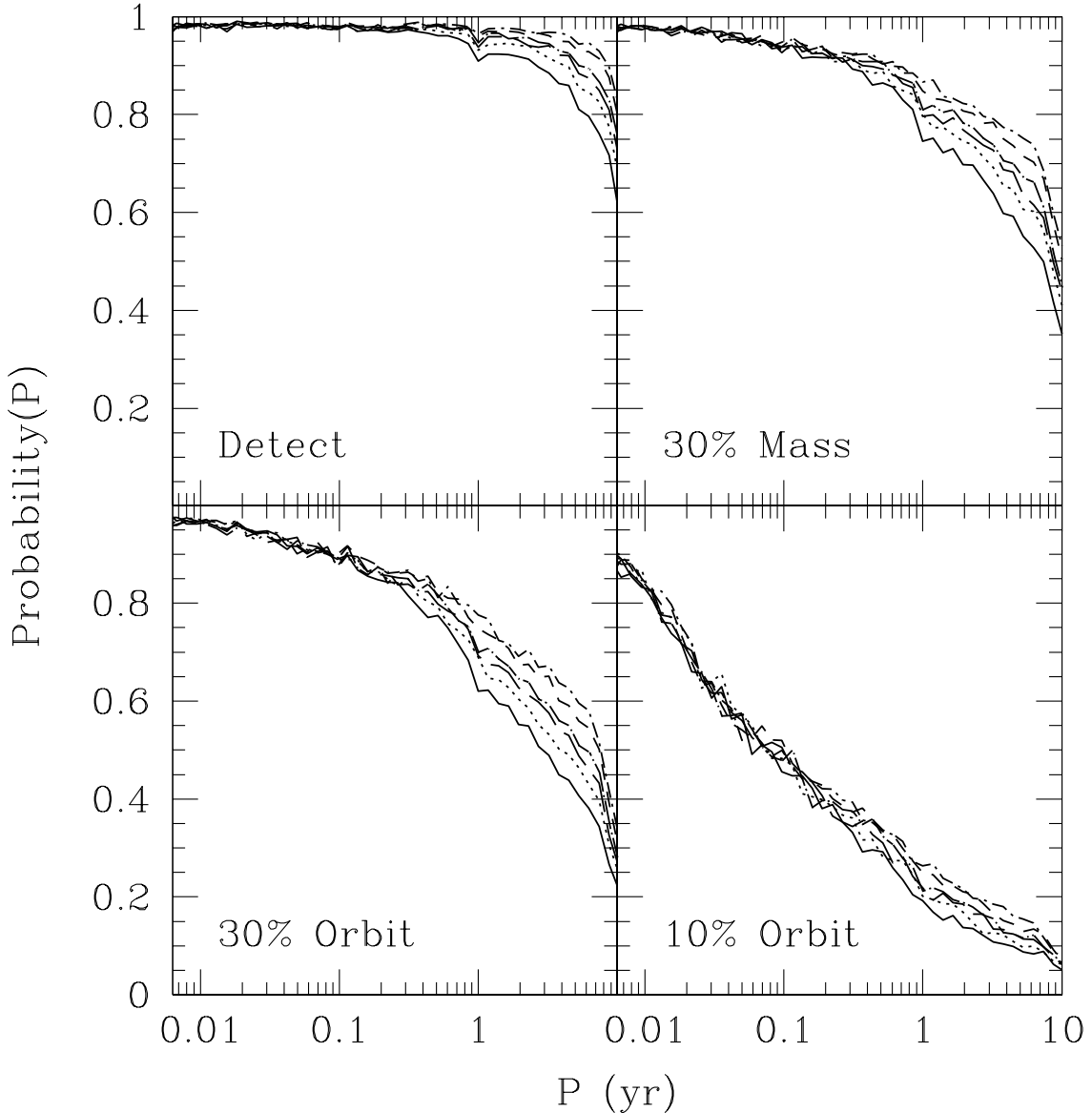


Fig. 7.— In each panel we show the probability for detecting a planet or measuring its mass or orbit as a function of the orbital period, P , for a fixed scaled signal, $S = 4$, averaging over the eccentricities, and other parameters. The upper left panel is for detecting a planet, the upper right panel is for measuring the mass with 30% accuracy, the lower left panel is for measuring the orbit with 30% accuracy, and the bottom right panel is for measuring the orbital parameters with 10% accuracy. The different line styles are for simulations using geometric observing schedules with different minimum spacings, Δt_{min} (solid, 1d; dotted, 3d; long dash, 6d; dot-long dash, 10d; short dash, 30d; dot-short dash, 60d). For orbital periods approaching the duration of the astrometric survey, the observing schedules with

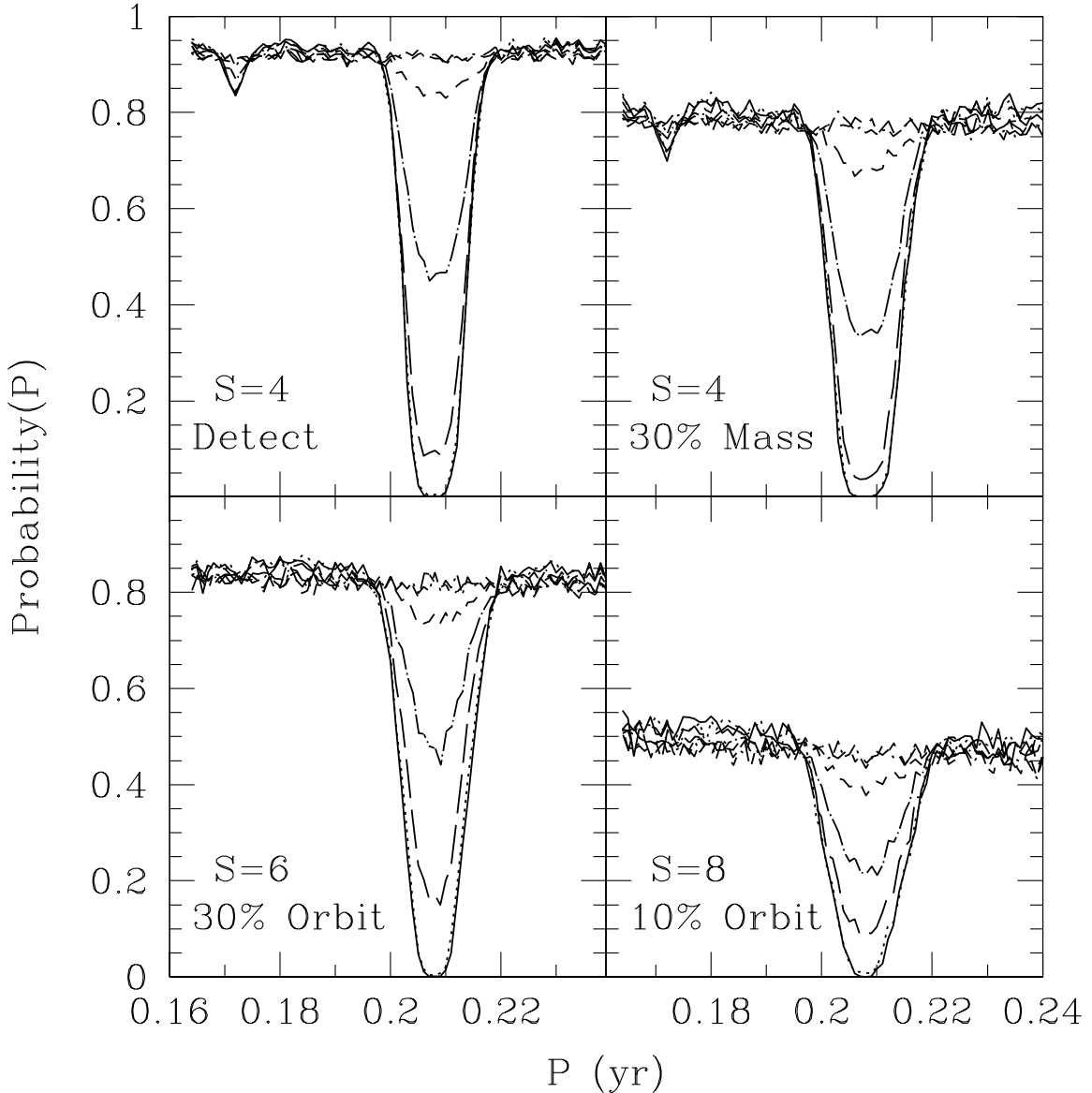


Fig. 8.— In each panel we show the probability for detecting a planet or measuring its mass or orbit as a function of the orbital period, P , for a fixed scaled signal, S , averaging over the other parameters. The upper left panel is for detecting a planet ($S = 4$), the upper right panel is for measuring the mass with 30% accuracy ($S = 4$), the lower left panel is for measuring the orbit with 30% accuracy ($S = 6$), and the bottom right panel is for measuring the orbital parameters with 10% accuracy ($S = 8$). The different line styles are for simulations using perturbations with different magnitudes, or values of ϵ (solid, $\epsilon = 0$, regular periodic; dotted, $\epsilon = 0.02$; dashed, $\epsilon = 0.05$; dot-long dash, $\epsilon = 0.1$; short dash, $\epsilon = 0.2$; dot-short dash, $\epsilon = 0.4$; short dash-long dash, $\epsilon = 0.6$). Perturbations with magnitudes

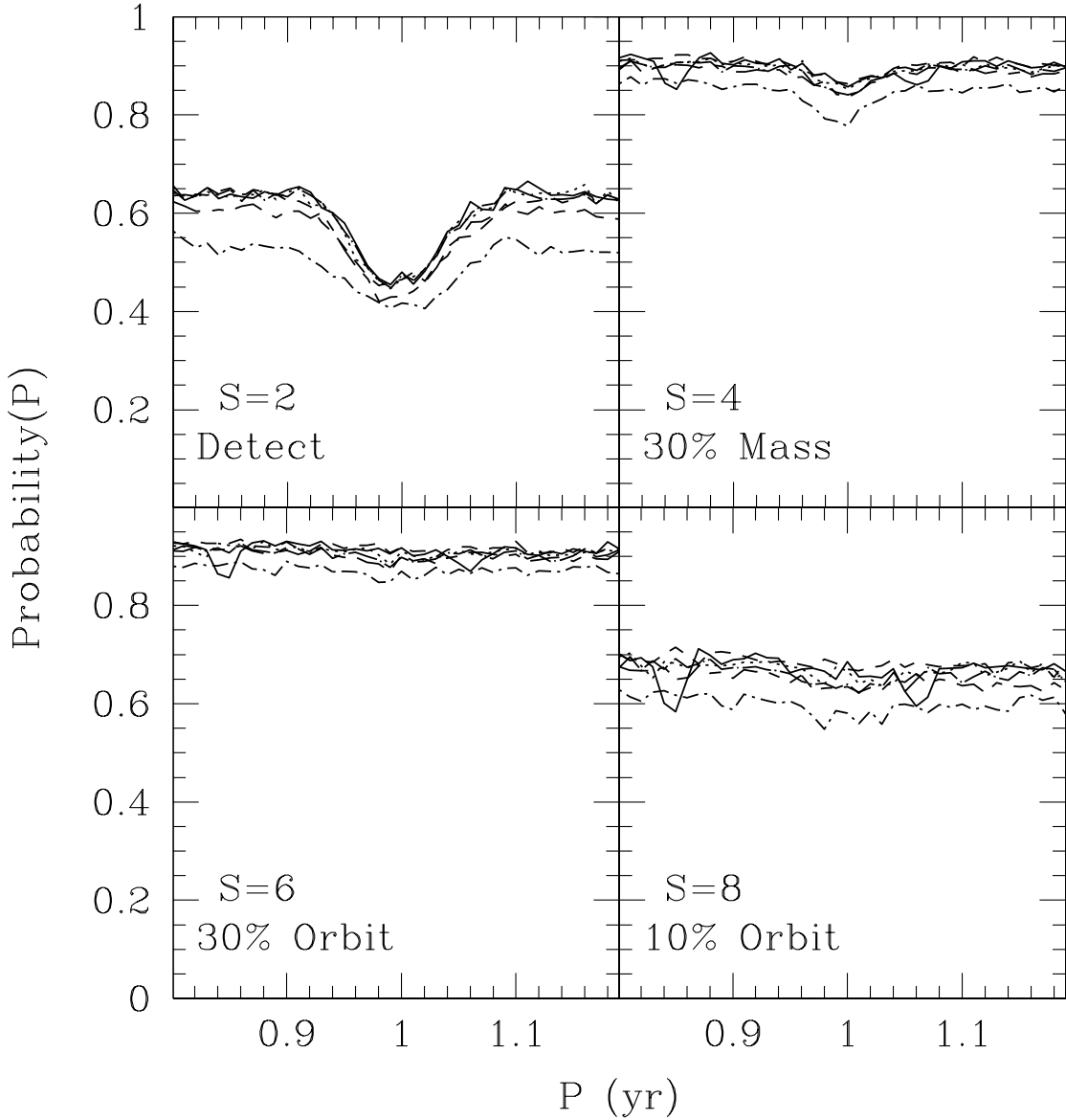


Fig. 9.— In each panel we show the probability for detecting a planet or measuring its mass or orbit as a function of the orbital period, P , for a fixed scaled signal, S , averaging over the other parameters. The upper left panel is for detecting a planet ($S = 2$), the upper right panel is for measuring the mass with 30% accuracy ($S = 4$), the lower left panel is for measuring the orbit with 30% accuracy ($S = 6$), and the bottom right panel is for measuring the orbital parameters with 10% accuracy ($S = 8$). The different line styles are for simulations using different observing schedules (solid, periodic; dotted, periodic with perturbations ($\epsilon = 0.2$); dot-long dash, logarithmic ($\Delta t_{min} = 30$ d); short dash, power law ($\beta = 0.5$); dot-short dash, geometric ($\Delta t_{min} = 30$ d); short dash-long dash, Golomb ruler). The choice of observing

Table 1. Rates of Detections and Measurements for All Planets

	Detections		Masses		Orbits	
	χ^2 -test	F-test	30%	10%	30%	10%
Regular Periodic	0.66	0.59	0.62	0.54	0.58	0.46
Random Uniform	0.66	0.59	0.61	0.53	0.57	0.45
Golomb Ruler	0.66	0.59	0.61	0.53	0.57	0.45
Periodic w/ Gaussian Perturbations						
$\epsilon = 0.05$	0.66	0.59	0.62	0.54	0.58	0.46
$\epsilon = 0.1$	0.66	0.59	0.62	0.54	0.58	0.46
$\epsilon = 0.2$	0.66	0.59	0.62	0.54	0.58	0.46
$\epsilon = 0.4$	0.66	0.59	0.62	0.54	0.58	0.46
Regular Logarithmic						
$\Delta t_{min} = 1$ d	0.63	0.56	0.59	0.51	0.55	0.43
$\Delta t_{min} = 3$ d	0.64	0.57	0.60	0.52	0.56	0.44
$\Delta t_{min} = 10$ d	0.65	0.59	0.61	0.53	0.57	0.45
$\Delta t_{min} = 30$ d	0.66	0.59	0.62	0.54	0.58	0.45
Random Logarithmic						
$\Delta t_{min} = 1$ d	0.60	0.53	0.55	0.48	0.52	0.40
$\Delta t_{min} = 3$ d	0.61	0.54	0.56	0.48	0.52	0.41
$\Delta t_{min} = 10$ d	0.62	0.55	0.58	0.50	0.54	0.42
$\Delta t_{min} = 30$ d	0.63	0.56	0.59	0.51	0.55	0.43

Note. — This table lists rates for detecting and characterizing planets with masses $1M_{\oplus}$ – $10M_{Jup}$ around stars at distances of 1 – 20pc. The first column lists the probability of rejecting the best-fit no-planet model based on a χ^2 -test. The second column lists the probability that the best-fit one-planet model significantly reduces χ^2 compared to the best-fit no-planet model according to an F -test. The remaining columns list the probabilities of measuring a planet’s mass and orbital parameters to within 30% and 10% of their actual values. The typical random uncertainty is less than 0.01.

Table 1. Cont.

	Detections		Masses		Orbits	
	χ^2 -test	F-test	30%	10%	30%	10%
Regular Power Law						
$\beta = 0.5$	0.65	0.58	0.61	0.53	0.58	0.46
$\beta = 1$	0.66	0.59	0.62	0.54	0.58	0.46
$\beta = 2$	0.66	0.59	0.62	0.53	0.58	0.45
Random Power Law						
$\beta = 0.5$	0.65	0.58	0.61	0.53	0.57	0.45
$\beta = 1$	0.64	0.57	0.60	0.52	0.56	0.45
$\beta = 2$	0.62	0.55	0.59	0.51	0.55	0.44
Regular Geometric						
$\Delta t_{min} = 1$ d	0.62	0.55	0.57	0.49	0.53	0.41
$\Delta t_{min} = 3$ d	0.63	0.56	0.58	0.50	0.54	0.42
$\Delta t_{min} = 10$ d	0.63	0.57	0.59	0.51	0.55	0.43
$\Delta t_{min} = 30$ d	0.64	0.58	0.60	0.52	0.56	0.44

Table 2. Rates of Detections and Measurements for Low Mass Planets

	Detections		Masses		Orbits	
	χ^2 -test	F-test	30%	10%	30%	10%
Regular Periodic	0.30	0.21	0.24	0.16	0.21	0.09
Random Uniform	0.29	0.20	0.23	0.15	0.19	0.08
Golomb Ruler	0.29	0.20	0.23	0.15	0.19	0.08
Periodic w/ Gaussian Perturbations						
$\epsilon = 0.05$	0.30	0.21	0.24	0.16	0.20	0.09
$\epsilon = 0.1$	0.30	0.21	0.24	0.16	0.20	0.09
$\epsilon = 0.2$	0.30	0.20	0.24	0.16	0.20	0.09
$\epsilon = 0.4$	0.30	0.20	0.24	0.16	0.20	0.09
Regular Logarithmic						
$\Delta t_{min} = 1$ d	0.25	0.16	0.18	0.11	0.15	0.06
$\Delta t_{min} = 3$ d	0.26	0.17	0.20	0.13	0.17	0.06
$\Delta t_{min} = 10$ d	0.28	0.19	0.22	0.14	0.19	0.08
$\Delta t_{min} = 30$ d	0.30	0.20	0.23	0.15	0.20	0.09
Random Logarithmic						
$\Delta t_{min} = 1$ d	0.21	0.13	0.15	0.09	0.12	0.04
$\Delta t_{min} = 3$ d	0.23	0.14	0.16	0.10	0.13	0.04
$\Delta t_{min} = 10$ d	0.24	0.15	0.18	0.11	0.14	0.05
$\Delta t_{min} = 30$ d	0.26	0.17	0.19	0.12	0.16	0.06

Note. — This table lists rates for detecting and characterizing planets with masses $1M_{\oplus}$ - $20M_{\oplus}$ around stars at distances of 1 – 20pc. The typical random uncertainty is less than 0.01.

Table 2. Cont.

	Detections		Masses		Orbits	
	χ^2 -test	F-test	30%	10%	30%	10%
Regular Power Law						
$\beta = 0.5$	0.30	0.20	0.24	0.16	0.20	0.08
$\beta = 1$	0.30	0.21	0.24	0.16	0.20	0.09
$\beta = 2$	0.29	0.20	0.23	0.15	0.20	0.08
Random Power Law						
$\beta = 0.5$	0.29	0.20	0.23	0.15	0.19	0.08
$\beta = 1$	0.29	0.19	0.23	0.15	0.19	0.07
$\beta = 2$	0.28	0.18	0.22	0.14	0.18	0.06
Regular Geometric						
$\Delta t_{min} = 1$ d	0.23	0.14	0.17	0.10	0.13	0.05
$\Delta t_{min} = 3$ d	0.24	0.15	0.18	0.11	0.15	0.05
$\Delta t_{min} = 10$ d	0.26	0.17	0.19	0.12	0.16	0.06
$\Delta t_{min} = 30$ d	0.27	0.18	0.20	0.13	0.17	0.07